Single-crystal Vibrational Spectra of Apatite, Vanadinite, and Mimetite

By **David M. Adams** * and **Ian R. Gardner**, Department of Chemistry, University of Leicester, Leicester LE1 7RH

Single-crystal Raman spectra are reported for the three title compounds, and i.r.-reflectance parameters for apatite. An essentially complete assignment is deduced for apatite, including lattice modes, and is in close agreement with the predictions of factor-group analysis. The main features of the Raman spectra of vanadinite and mimetite are similarly accounted for. Factors causing broadening of some low-frequency Raman bands are discussed.

MUCH effort has been devoted to i.r. and, to a lesser extent, Raman spectroscopy of minerals, but extraordinarily little of this work has been done with oriented single crystals. Of the minerals structurally related to fluorapatite, $Ca_5(PO_4)_3F$, this end-member has been the most extensively investigated, partly due to its importance in bones and teeth. It also presents a substantial spectroscopic challenge as the primitive cell has 126 normal vibrations of which 54 arise from coupling of six phosphate ions, and a further 72 are lattice modes. Spectra of this complexity can be elucidated and assigned only by using the methods of single-crystal spectroscopy. There have been many qualitative studies of vibrational spectra of apatites, but the only single-crystal work reported prior to ours is that of Kravitz *et al.*[1] who made a detailed practical and theoretical investigation of the phosphate vibrational interactions using both Raman and i.r.-reflectance spectroscopy. We have extended this work to include the low-frequency region, and have also included the related minerals vanadinite, $Pb_5(VO_4)_3Cl$, and mimetite, $Pb_5(AsO_4)_3Cl$, in an attempt to further understanding of the whole group of spectra. No single-crystal work has been reported previously for vanadinite and mimetite. After completion of our work two further single-crystal papers on apatite appeared, one [2] essentially repeating the experimental work of Kravitz *et al.*, the other [3] being a partial Raman study; we discuss them below.

EXPERIMENTAL

Raman spectra were recorded at room temperature using Coderg T800 (triple-monochromator) and PH1 (double-monochromator) instruments. Argon-ion and helium–neon exciting lines were used as shown in Table 1. I.r.-reflectance spectra were recorded because (*a*) the specimens must not be damaged and (*b*) it would be difficult, if not impossible, to cut thin enough sections for transmission spectroscopy. For the region 20—800 cm^{-1} a Beckman–R.I.I.C. FS-720 Fourier spectrometer with RS7F reflectance module was used. A Perkin-Elmer 225 instrument was used for the 400—10 000 cm^{-1} interval, with the reflectance accessory reported earlier.[4] Wire-grid polarisers were employed. Kramers–Krönig analysis of the reflectance spectra yielded the parameters ε', ε'', n, and k where the complex dielectric constant $\varepsilon^* = \varepsilon' - i\varepsilon'' = (n^*)^2$ and $n^* = n - ik$.

Crystal specimens were obtained from the British Museum, and Dr. King of the Geology Department, University of Leicester, as detailed in Table 1.

[1] L. C. Kravitz, J. D. Kingsley, and E. L. Elkin, *J. Chem. Phys.*, 1968, **49**, 4600.

[2] D. K. Arkhipenko, B. A. Orekhov, and R. G. Knubovets, *Optics and Spectroscopy*, 1973, **34**, 737.

[3] I. I. Shaganov and V. S. Libov, *Optics and Spectroscopy*, 1973, **35**, 181.

[4] D. M. Adams and M. M. Hargreave, *J.C.S. Dalton*, 1973, 1426.

Selection Rules.—Fluorapatite belongs to the hexagonal system, $C_{6h}^2 \equiv P6_3/m$, with $z = 2$. The factor-group analysis (f.g.a.) is shown in Table 2, together with a correlation diagram for the anion internal modes. Fluorine is

TABLE 1

The minerals used, their provenance, and laser lines used for excitation of their Raman spectra

Mineral	Source	Collection and accession no.	Wavelength of laser line/nm
Apatite	Durango, Mexico	Leicester University, Geology Dept., 20612	514·5
Apatite	Mt. Apatite, Maine	BM 87031	488·0
Vanadinite	Yuma County, Arizona	BM 6441	632·8
Vanadinite	Hillsboro, New Mexico	BM 83397	514·5
Mimetite	Wheal Alfred, Cornwall	BM 33085	514·5

BM = British Museum.

TABLE 2

Vibrational selection rules for fluorapatite, $Ca_5F(PO_4)_3$

	N_{opt}	T	R	N_{int}	Activities
A_g	12	5	1	6	Raman: $x^2 + y^2$; z^2
B_g	9(8) [a]	4(3)	2	3	
E_{1g}	8	3	2	3	Raman: (yz, zx)
E_{2g}	13(12)	6(5)	1	6	Raman: $(x^2 - y^2, xy)$
A_u	8	3	2	3	I.r.: z
B_u	12(13)	5(6)	1	6	
E_{1u}	12	5	1	6	I.r.: (x, y)
E_{2u}	8(9)	3(4)	2	3	

Correlation scheme

Free ion, T_d	Site, C_s	×6 → Crystal, C_{6h}^2
ν_1 a_1 ν(P–O)	a'	
ν_2 e δ(P–O)	$a' + a''$	$6a'$ → $6(A_g + E_{2g} + B_u + E_{1u})$
ν_3 t_2 ν(P–O)	$2a' + a''$	$3a''$ → $3(B_g + E_{1g} + A_u + E_{2u})$
ν_4 t_2 δ(P–O)	$2a' + a''$	

N_{opt}, T, R, and N_{int} are the number of optical, optic-branch translatory, phosphate rotatory, and coupled phosphate internal modes, respectively.

[a] Numbers in parentheses refer to vanadinite and mimetite (see text).

in Wyckoff sites 2*a* in apatite; in mimetite and vanadinite chlorine occupies sites 2*b*. These atoms contribute the following vectors to the f.g.a.: [5]

F on 2*a*	0	1	0	1	1	0	1	0
Cl on 2*b*	0	0	0	0	1	1	1	1

Here the order of symmetry species is that of Table 2. Thus, only the translational part of the lattice-mode spectrum is affected and the only optically active species involved is E_{2g}. The selection rules for all three minerals are therefore identical with the single exception that vanadinite and mimetite show one *less* lattice mode of type E_{2g} than does apatite.

RESULTS AND DISCUSSION

Our i.r.-reflectance results for the phosphate region of apatite are in good agreement with those of Kravitz *et al.*[1] In addition, we give the low-frequency spectra and values of l.o. mode frequencies determined from $|\varepsilon|$,[6] and have analysed observed A_u and E_{1u} reflectance

[5] D. M. Adams and D. C. Newton, ' Tables for Factor Group and Point Group Analysis,' Beckman–R.I.I.C. Limited, Croydon, 1970.

TABLE 3

L.o. and t.o. mode wavenumbers (cm^{-1}) for fluorapatite as determined from i.r.-reflectance spectra. Values in parentheses (A_u modes only) were estimated visually (see text), others being obtained by Kramers–Krönig analysis; those from refs. 1 and 3 were obtained by classical harmonic-oscillator analyses

A_u				E_{1u}				
l.o.	t.o.			l.o.	t.o.			
	a	*b*	*c*	*a*	*a*	*b*	*c*	
108	96			115	100			Lattice modes
(102)	(96)							
193	184			204	193			
(190)	(178)							
d	277			*d*	224			
	(267)							
342	304			255	243			
(360)	(296)							
				296	273			
				386	327			
624	582	563	559	588	580	573	575	ν_2, ν_3
(604)	(570)							
				624	604	595	598	
1 120	1 030	1 034	1 030	1 072	1 034	1 037	1 043	ν_1, ν_3
(1 124)	(1 028)							
				1 120	1 094	1 092	1 091	

l.o. and t.o. = Longitudinal and transverse optics.

[a] This work. [b] Ref. 3. [c] Ref. 1. [d] Not obtained due to bands overlapping.

spectra by the Kramers–Krönig procedure (Table 3 and Figure 1). Even without an analysis, approximate t.o. and l.o. mode frequencies can be read from the observed reflectance spectra because a reflectance band is bounded on the low-frequency side by the t.o. mode, and on the high-frequency side by the l.o. mode. For the E_{1u} species our Kramers–Krönig analysis yielded t.o. and l.o. frequencies close to where they are expected, but for the A_u species the values were too high by up to 10 cm^{-1}. This is not an uncommon experience with Kramers–Krönig analysis; indeed the literature is full of pained comments about its unaccountable failures. There is some evidence that errors of this kind are more probable in crowded spectra, but in this case the E_{1u} spectrum is more crowded than that from A_u modes. We therefore include, in Table 3, A_u frequencies estimated visually from the reflectance spectra. Both Kravitz *et al.*[1] and the authors of ref. 3 analysed their reflectance spectra using the classical harmonic-oscillator model; the former authors used this method because of difficulties with Kramers–Krönig analysis. Their results are in good mutual agreement but show some small differences from ours which are probably within the limits of error of the analyses. Comparison of l.o.–t.o. splittings with intensity values at ε''(max) shows them to be in good qualitative agreement.

The Raman spectra showed excellent extinctions (Figure 2). In aqueous solution the Raman spectrum of the ion $[PO_4]^{3-}$ showed four lines (Table 4); apatite showed Raman and i.r. activity close to these four regions, indicating that bands observed below 400 cm^{-1} are associated with lattice modes. Assignment of the

[6] S. Nudelman and S. S. Mitra, ' Optical Properties of Solids,' Plenum, New York, 1969.

phosphate internal modes for apatite follows directly from the results and selection rules and is summarised in Table 4. From this we conclude that physical interactions between the six phosphate groups in the primitive cell are strong enough to yield the full splitting scheme described by f.g.a. Not all the formally allowed modes were observed because of the intrinsic weakness of some of them. Thus, Raman-active $\nu_1(a_1)$ of the ion $[PO_4]^{3-}$ may develop i.r.-activity by virtue of site and correlation fields, but these mechanisms do not provide enough intensity for the i.r.-active components to be observed, although Raman-active components were readily seen. The same is true of ν_2. In contrast, $\nu_3(t_2)$ begins with both i.r. and Raman activity and gives rise to the full predicted splitting scheme, from which values of the site frequencies may be estimated (shown in parentheses). For all four anion modes, ν_1—ν_4, the splitting effect of the site field was at least twice that of the correlation field. For ν_1 and ν_2 solution wavenumbers were raised *ca.* 20 cm^{-1} by the site field (the corresponding value for ν_3 and ν_4 is *ca.* 30 cm^{-1}) and then

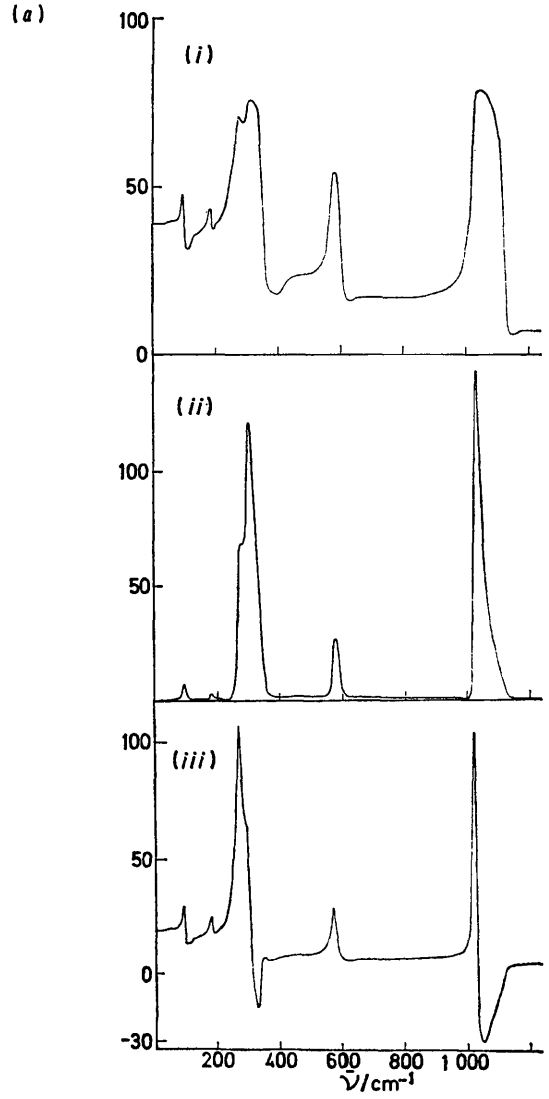

FIGURE 1(*a*)

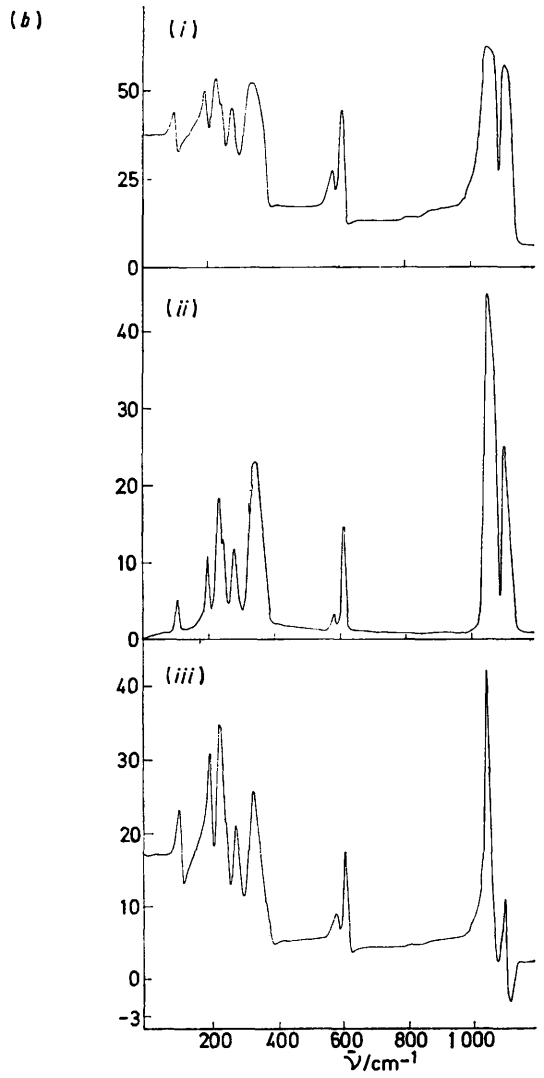

FIGURE 1 I.r. reflectance spectrum of fluorapatite: (*a*) A_u; (*b*) E_{1u} species. Each figure shows: (*i*), the observed percentage reflectance spectrum; (*iii*) and (*ii*), real (ε') and imaginary (ε'') parts of the complex dielectric constant, calculated by Kramers–Krönig analysis

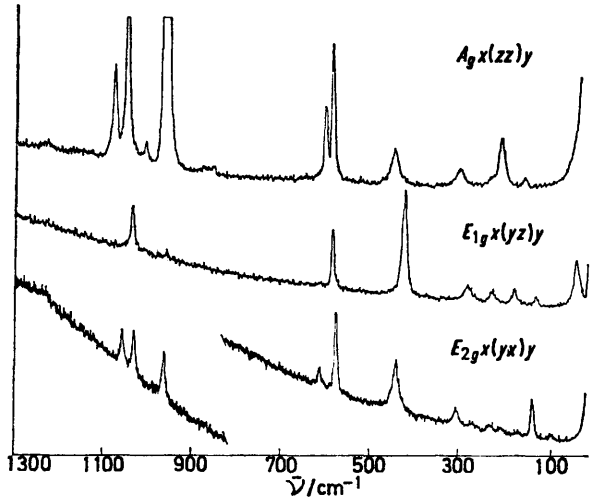

FIGURE 2 Raman spectrum of fluorapatite: spectral slit width 2 cm^{-1}; 514·5 nm excitation, *ca.* 100 mW at the sample

TABLE 4

Raman wavenumbers (cm^{-1}) and intensities (in parentheses, arbitrary scale) for single-crystal apatite: (*a*) the coupling of $[PO_4]^{3-}$ modes (wavenumbers in square brackets are degeneracy-weighted averages); (*b*) the lattice modes

(*a*) Ion in aqueous solution,[4] T_d → Site, C_s → Crystal, C_{6h}^2

ν_1, a_1	938	A'		A_g 963(500) E_{2g} 965(25) E_{1u}
ν_2, e	420	A' [448] [a] A'' [430] [a]		A_g 452(17) E_{2g} 445(28) E_{1u}
			E_{1g} 431(67) A_u	
ν_3, t_2	1 017	$2A'$ [1 037, 1077] A'' [1 037]		$2A_g$ 1 051(150), 1 080(59) $2E_{2g}$ 1 033(23), 1 058(20) $2E_{1u}$ 1 034, 1 094
			E_{1g} 1 040(22) A_u 1 030	
ν_4, t_2	567	$2A'$ [583, 614] A'' [588]		$2A_g$ 591(80), 607(45) $2E_{2g}$ 581(47), 617(8) $2E_{1u}$ 580, 614
			E_{1g} 591(32) A_u 582	

[a] The effect of missing A_u and E_{1u} vibrations has been neglected.

(*b*) Lattice modes (relative intensities in parentheses):

$x(zz)y$ A_g	$x(yz)y$ E_{1g}	$x(yz)y$ E_{2g}
160(5)	44(27)	100(6)
212(30)	135(5)	139(24)
231(8)	183(9)	177(4)
306(10)	233(6)	214(4)
	289(9)	237(5)
		277(4)
		311(10)

TABLE 5

Raman wavenumbers (cm^{-1}) and intensities (arbitrary scale) for vanadinite (Yuma sample) and mimetite

Vanadinite					Mimetite				
		$x(zz)y$	$x(yz)y$	$x(yx)y$			$x(zz)y$	$x(yz)y$	$x(yz)y$
E_{1g}	33		98		A_g	32	23		
A_g	45	500	50		E_{1g}	36		15	
A_g	87	53			A_g	49	50		
E_{2g}	98			60					
E_{1g}	104		27		E_{1g}, E_{2g}	50		19	40
A_g	149	54			A_g	91	30		
E_{2g}	167			16					
E_{1g}	178		10		E_{1g}	100		7	4
A_g	181	25			A_g	102	27	7	
E_{2g}	185			10	A_g	170	12		
					E_{1g}	181		3	
A_g	294	95			A_g	306	7		
A_g	324	27			E_{1g}	313		6	
E_{1g}	326		97						
E_{2g}	328			(sh)					
E_{2g}	334			30	A_g	338	12		
E_{2g}	356			41	E_{1g}	340		4	
A_g	371	120			A_g	390	4		
					A_g	410	8	2	
					A_g	428	4		
A_g	725	21			A_g	765	8		
E_{2g}	795	1	6	33	E_{1g}	785		3	
A_g	828	270	20	50	A_g, E_{2g}	808	60	7	6
					$A_g, (E_{2g})$	814	90	7	4

split about this value by both site and correlation effects. Our Raman results are in good agreement with those of Kravitz *et al.*, but the Russian work [3] suffers from poor extinctions between orientations and is at low resolution; they therefore missed several bands found both by ourselves and Kravitz *et al.*

Aqueous-solution frequencies for vanadate and arsenate show that for both ions ν_1 and ν_3 are in near coincidence, as are ν_2 and ν_4. Four clear regions of activity due to phosphate in apatite were reduced in vanadinite and mimetite to two complex regions, ν(E–O) and δ(E–O), in which it is impossible to disentangle individual contributions from ν_1 and ν_3, and ν_2 and ν_4; indeed, such a procedure would be meaningless as there must be Fermi resonance. Good Raman data were obtained for vanadinite and mimetite (Table 5), but the crystals were too small to permit determination of their i.r.-reflectance spectra. Since these minerals contain heavier components than apatite their lattice modes must be at *lower* frequencies. Both showed a complex set of emissions below 180 cm^{-1} but there was then a clear gap up to *ca.* 300 cm^{-1}. We conclude that modes in the 300—430 cm^{-1} region are associated with ν_2 and ν_4 components of the ions $[VO_4]^{3-}$ and $[AsO_4]^{3-}$,

and are automatically led to the assignment shown in Table 6 for vanadinite.

TABLE 6

Assignments for factor-group components (cm^{-1}) of the ions $[VO_4]^{3-}$ and $[AsO_4]^{3-}$ in vanadinite and mimetite

Ion, T_d		Crystal, C_{6h}^2	Vanadinite (Yuma)			Mimetite		
$\nu_1\ a_1$		$3A_g$	828	725		814	808	765
$\nu_3\ t_2$	→	E_{1g}				785		
		$3E_{2g}$	828	795		(814)	806	
$\nu_2\ e$		$3A_g$	371	324	294	410	338	306
$\nu_4\ t_2$	→	$2E_{1g}$	326			340	313	
		$3E_{2g}$	356	334	328			

In accord with the known high bond polarisability of the ion $[VO_4]^{3-}$, vanadinite exhibited an extremely intense A_g ν(V=O) mode but, in severe contrast, developed no intensity in this region of the E_{1g} spectrum although there *was* a strong line in the δ(OVO) region at 326 cm^{-1}. Observation of nearly the full factor-group splitting in the ν_2,ν_4 region implies that lack of such splitting in the ν_1,ν_3 region is due to accidental weakness rather than to weak site and correlation fields. The mimetite spectra are less readily interpreted. The quality of the Raman extinctions was relatively poor and we suspect that this specimen is not an end-member; for example, the ν_2,ν_4 region showed more than the predicted number of lines. The E_{2g} spectrum was also exceptionally weak and nothing was observed between 110 and 750 cm^{-1}. Nevertheless, the partial assignment given in Table 6 suggests that this crystal also exhibits full factor-group splitting.

Lattice Modes.—For apatite 10 of the 11 predicted i.r.-active lattice modes and 16 of the 18 Raman lattice modes were observed. There was no evidence on which to base a division into translatory and rotatory modes even supposing such a distinction is valid in this case which is doubtful. However, it is probable that the sole Raman-active lattice mode associated with the fluoride ion is to be associated with the E_{2g} line at 311 cm^{-1}, as this will be the highest of the lattice modes. Vanadinite and mimetite do not show an equivalent band due to chloride ion as the selection rules show that chloride motion does not contribute to the Raman spectrum. In the Raman spectra of vanadinite and mimetite, lattice modes were crowded together in the region below 180 cm^{-1} (due partly to increased masses, and to the decrease in bond strength from Ca–O to Pb–O) and accidental degeneracies are to be expected. Since these two minerals differ only in having V or As atoms, their low-frequency spectra were naturally very similar. In seeking to compare theory with experiment we are faced with two further problems in the low-frequency region: (*a*) are any of the bands due to second-order processes?; (*b*) is the pronounced breadth of some of the bands due to isomorphous replacement in the mineral, to near-accidental degeneracy, or to some other cause?

All three minerals showed several broad bands at low frequencies, but the problem is raised in an acute form in the E_{2g} spectrum of vanadinite (Figure 3), which exhibited particularly broad and rather featureless emission in the 130—190 cm^{-1} interval, along with other bands of normal appearance. Isomorphous replacement will lead to band broadening chiefly by reducing the translational symmetry of the lattice. The Raman process samples optical phonons with wave vectors $k \approx 0$. If translational symmetry is reduced the scattering phonon can in principle take any value $k \neq 0$ in the Brillouin zone, since conservation of wave vector is no longer required, thereby generating broad bands. In the absence of data from pure synthetic analogues it is not possible to disentangle the causes of the band broadening observed, and hence impossible to

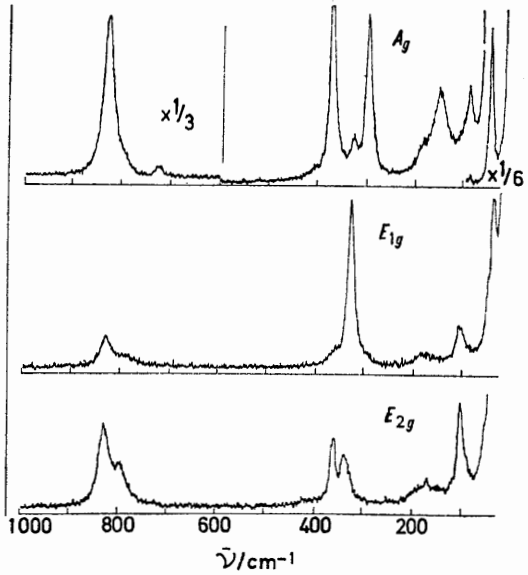

FIGURE 3 Raman spectrum of vanadinite (Yuma sample): spectral slit width 2 cm^{-1}; 632·8 nm excitation, *ca.* 15 mW at the sample

know how many first-order bands are present. However, for apatite the broadening was not very pronounced and we tentatively attribute all observed bands to lattice modes. For vanadinite the number of bands present at least approached that predicted by f.g.a., whilst interpretation of the mimetite spectra is not pursued due to its doubtful composition. We note, finally, that, of our two samples of vanadinite, the Hillsboro one showed a rather more complex Raman spectrum in the ν(V=O) region; the additional bands correspond quite well with the principal ones of mimetite implying that some $[AsO_4]^{3-}$ ions are substituted for $[VO_4]^{3-}$. However, in the low-frequency region, although the lattice-mode spectra showed a few more lines than in the Yuma sample, they were not noticeably different in breadth. This could be taken to imply that second-order processes are the main cause of the broad features discussed above.

We thank Dr. P. G. Embrey and Mr. J. P. Fuller of the British Museum (Natural History) for their help in selection of mineral samples and the S.R.C. for an award (to I. R. G.).

[4/208 *Received, 4th February,* 1974]